applied sciences

MDPI

Article

Optimization of Brake Calipers Using Topology Optimization for Additive Manufacturing

Evangelos Tyflopoulos *, Mathias Lien and Martin Steinert

Department of Mechanical and Industrial Engineering, Norwegian University of Science and Technology (NTNU), 7491 Trondheim, Norway; mathias.lien1997@gmail.com (M.L.); martin.steinert@ntnu.no (M.S.)

* Correspondence: evangelos.tyflopoulos@ntnu.no; Tel.: +47-7341-262-3

Abstract: The weight optimization of a structure can be conducted by using fewer and downsized components, applying lighter materials in production, and removing unwanted material. Topology optimization (TO) is one of the most implemented material removal processes. In addition, when it is oriented towards additive manufacturing (AM), it increases design flexibility. The traditional optimization approach is the compliance optimization, where the material layout of a structure is optimized by minimizing its overall compliance. However, TO, in its current state of the art, is mainly used for design inspiration and not for manufacturing due to design complexities and lack of accuracy of its design solutions. The authors, in this research paper, explore the benefits and the limitations of the TO using as a case study the housings of a front and a rear brake caliper. The calipers were optimized for weight reduction by implementing the aforementioned optimization procedure. Their housings were topologically optimized, partially redesigned, prepared for 3D printing, validated, and 3D printed in titanium using selective laser melting (SLM). The weight of the optimized calipers reduced by 41.6% compared to commercial calipers. Designers interested in either TO or in automotive engineering can exploit the findings in this paper.

Keywords: topology optimization; additive manufacturing; brake caliper

Citation: Tyflopoulos, E.; Lien, M.; Steinert, M. Optimization of Brake Calipers Using Topology Optimization for Additive Manufacturing. *Appl. Sci.* **2021**, *11*, 1437. https://doi.org/10.3390/app11041437

Academic Editor: Cem Selcuk
Received: 5 January 2021
Accepted: 28 January 2021
Published: 5 February 2021

1. Introduction

The reduction of car weight is a topic of high importance in the automotive industry. A lighter car has an increased acceleration, and thus an improved performance. Moreover, this weight reduction reduces material cost, improves fuel efficiency, as well as reduces vehicle exhaust emissions. According to Li, et al. [1], for every 100 kg weight reduction of light transport vehicles (LTV), their fuel consumption will be decreased on average by approximately 0.4 L/100 km, and thus their CO_2 emissions will be mitigated by 8–11 g/km. There are several ways to reduce car weight, such as the use of lighter materials in manufacturing, the downsizing of the car, and the removal of unwanted material from car components [2]. One of the most implemented material-removal methods is topology optimization (TO).

TO is a popular optimization procedure that is applied for both research and manufacturing purposes. It is a mathematical method that optimizes the distribution of the material spatially in a design domain under the given objective functions, boundary conditions, and constraints. This can result in significant material savings of the structures while their mechanical strength is either maintained or enhanced. The TO, together with the size and shape optimization, constitute the three categories of the so-called structural optimization (SO) [3]. The most common approaches for solving the TO-problem are the Solid Isotropic Material with Penalization (SIMP), the Bidirectional Evolutionary Structural Optimization (BESO), and the level-set based optimization [4]. A description of the TO problem along with the SIMP approach that was applied in this research work is presented thoroughly in Section 2.

In general, TO finds many applications in the automotive industry and in mechanics, where the weight savings can be remarkable. The car doors, the suspension systems, and the brake systems are some of the most common topologically optimized components in literature. One of the first publications on TO applications in the automotive industry is the work of Yang and Chahande [5]. In their research paper, they optimized three models, including a truck frame, a deck lid, and a space frame structure, by using the traditional compliance TO method with an in-house TO software in Ford Motor Company. Another worth mentioning example is the optimization of the automotive tailor-welded blank door either by Shin, et al. [6] or by Li, et al. [7]. Shin, et al. [6] applied compliance TO in the first place, followed by a size/shape optimization, while Li, et al. [7] utilized the benefits from the BESO. Kong, et al. [8] optimized a spring lower seat from a suspension system by using a topology and topography optimization approach. Li and Kim [9] conducted multi-material compliance TO with SIMP as an interpolation method of an engine cradle and a cross-member of a chassis frame. Cavazzuti, et al. [10], in their study, optimized a Ferrari F458 chassis with the SIMP method. A conceptual design of an engine cradle was developed by Li, et al. [1] using a combined size, shape, and compliance TO. Sudin, et al. [2] applied the SIMP method to optimize the mass of a brake pedal. Concerning the optimization of brake calipers, only a few works are found in the literature. Mastinu [11] optimized both the brake caliper and the upright of a racecar with compliance TO. Ballo, et al. [12] developed a lightweight design of brake caliper implementing the SIMP approach. Farias, et al. [13] optimized a brake caliper in order to reduce both its weight and its heat transfer. On the other hand, Soh and Yoo [14] optimized the shape of a brake caliper for squeal noise reduction. Finally, Sergent, et al. [15] optimized the mass of an opposed piston brake.

The optimized structures in all these examples are characterized by their considerable weight savings or/and their performance improvements compared to their initials designs. However, the majority of the presented design solutions were conceptual numerical designs and not manufactured parts. It seems that TO in its current state of the art is mainly used for design inspiration and not for production [4]. The optimized parts are characterized by their design complexities, which make AM with 3D printing the most appropriate manufacturing method for them. A thorough review of TO for AM is presented in the recent research work of Zhu, et al. [16]. On the other hand, the redesign of the optimized designs contributes to the overcoming of these complexities and makes their manufacturing feasible by the conventional manufacturing processes (CMP). In addition, it and can eliminate possible overhangs at the 3D-printing parts. However, it can be time-consuming and, in some cases, challenging. In addition, the 3D printed parts can contain discrepancies compared to the numerical solutions.

The scope of this research work is to apply the TO in a real automotive component in order to identify benefits, challenges, limitations, as well as trade-offs in its implementation in the overall product development process, from an idea to an end product. For this reason, a case study of a front and a rear caliper, intended for a student racecar, is presented here. The brake calipers were designed, optimized, validated, as well as 3D printed in titanium with selective laser melting (SLM). A comparison between the numerical and the manufactured components contributed to the identification of possible deviations of the 3D printed parts. Designers and engineers interested in TO, AM, and automotive engineering can exploit the results of this research paper.

The rest part of the paper is composed as follows: In Section 2, the general TO problem, together with the SIMP method, is introduced. The essential theory about brake calipers is described in Section 3. The applied methodology in this research work is presented thoroughly in Section 4, while Section 5 includes the results of the optimized calipers. In Section 5, the challenges in the implementation of TO in manufacturing are discussed based on the findings in this paper. Finally, Sections 6 and 7 present the most important conclusions and the possible research possibilities, respectively.

2. The General Structural Optimization Problem and the SIMP Approach

At the general structural optimization (*SO*) problem, an objective function of a structure, f(x), such as manufacturing cost, strain energy, stress, and displacement, to mention a few, should be either minimized or maximized with respect to the given boundary conditions (equilibrium constraints), behavioral, and design constraints. Hence, the optimization problem can be described as [17]:

$$(SO)\begin{cases} minimize/maximize\ f(x,y)\ with\ respect\ to\ x\ and\ y \\ subject\ to\begin{cases} behavioral\ constraints\ on\ y \\ design\ constraints\ on\ x \\ equilibrium\ constraints. \end{cases} \end{cases} \quad (1)$$

In the case of a density-based TO problem of a structure, its design domain Ω is discretized to finite elements. A binary value is assigned to their density ρ_e; 1 for required material, and 0 for void. Hence, the nested mathematical formulation, based on the homogenization theory developed by Bendsøe [18], is the following:

$$\min F = F(u(\rho_e), \rho_e) = \int_{\Omega} f(u(\rho_e), \rho_e) dV \quad (2)$$

$$s.t.\ \ G_0(\rho_e) = \int_{\Omega} \rho_e dV - V_0 \leq 0 G_j(u(\rho_e), \rho_e) \leq 0 \text{ with j } = 1, \ldots, \text{m}$$

The $f(u(\rho_e), \rho_e)$ is the objective function, the ρ_e, in the state function $u(\rho_e)$, is the density of each element in the design domain Ω. $G_j(u(\rho_e), \rho_e)$ are the constraints, and V is the total volume of the structure. The most implemented objective function is the compliance of a structure. Compliance is the reciprocal of the stiffness, so in other words, by minimizing the compliance, the stiffness of the structure is increased.

The most challenging part of the solution of the TO problem is the calculation of the elastic modulus. The homogenization theory uses an effective elasticity tensor to describe the mesotropic properties of a structure [19]. The above formulation of a discrete TO problem resulted in the known "checkerboard" structural problem [20]. Solving the TO with continuous variables by interpolation could overcome this limitation. A popular interpolation method is the SIMP [21]. According to SIMP, the overall elasticity of a structure is calculated by the following formula:

$$E(\rho_e) = \rho_e^p E_0 \text{ with } p \geq 1 \text{ and } 0 < \rho_{min} \leq \rho_e \leq 1 \quad (3)$$

In this case, a continuous value is assigned to the elements' density, ρ_e. Furthermore, a minimum density $\rho_{min} \neq 0$ was used as a lower bound of density in order to avoid a calculation of a zero structure's elasticity. The "penalization" of the intermediate finite elements; elements with density $\rho_{min} < \rho_e < 1$ is conducted by the penalty factor, p. In other words, the SIMP method prevents the formation of the intermediate elements by increasing the structure's density to an exponent equal to p. According to Sigmund (2001), the ideal value of the penalty factor is three. Hence, the introduction of this factor reduces the elasticity, and in turn, the global stiffness is reduced.

Allaire, et al. [19] argue that SIMP is an over-simplified version of the initial homogenization theory and does not consider anisotropy. Despite this fact, the SIMP method is broadly implemented due to its simplicity. A plethora of different commercial software, software modules, as well as off the self-algorithms, has developed in the last decades in parallel with the continuous development of computational power in order to solve SO problems. The majority of these tools are still based on the traditional compliance TO-theory. The SIMP approach will also be applied in this research work.

3. Brake Calipers

A brake system is responsible for the deceleration of a vehicle, and thus is a vital part of driver's safety. The brake system is designed to both slow down and halt a vehicle by transforming its kinetic energy into heat while applying friction forces to the vehicle axles [22]. The most common brake system is the disc brake, which was initially developed in 1951 for racecars application. Just a few years later, in 1955, disc brakes were first used for mass production in the automotive industry, due to their success, on the Citroen DS model [23]. The disc brakes are steadily replacing drum brakes in order to overcome the potential brake power loss of the latter, also known as brake fade [22]. The most crucial component of a disc brake is the caliper that presses a pair of brake pads against the brake's disc, also called rotor, and thus slows down their rotational speed. In the case of hydraulic disc brakes, when the driver pushes the brake pedal, hydraulic pressure is applied by the brake fluid on the caliper's one or several pistons, and these, in turn, force the pads against the disc [24]. Figure 1 depicts a disc brake.

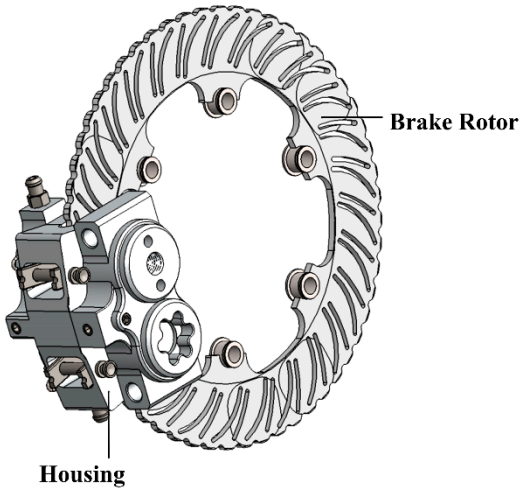

Figure 1. A 3D model of a disc brake design in SolidWorks.

The design of calipers is challenging and should be developed with respect to some technical requirements. According to Farias, et al. [13], the calipers must be stiff, light, and heat-resistant. Brake calipers require acceptable stresses and deflections under multiple load cases. It is important to mention that any crack on a caliper can lead to an instant brake fluid leak that results in brake malfunction. Thus, a high caliper stiffness provides a uniform pressure distribution on the brake system, which ensures short brake pedal travel, ride quality, and vehicle safety [15]. The term unsprung mass is broadly used to describe the total mass of the suspension, wheels, as well as other components connected to them. On the other hand, sprung mass consists of the supported by the suspension vehicle's body and components. In the case that the vehicle's brakes are mounted outboard, they are considered part of its unsprung mass [12]. As has already been mentioned, a minimization of the vehicle's mass increases its performance. Therefore, the reduction of brake caliper mass is of high importance. The applied friction forces between the brake pads and the rotor result in heat concentration inside the brake system. A low thermal resistance, together with insufficient ventilation of the brakes, increases their thermal deformations resulting in a smaller friction coefficient and, in turn, less braking force [13]. It seems that compliance TO of the brake calipers could reduce their weight while increasing their stiffness. Moreover, the creation of voids in the calipers' structure will increase their ventilation and heat dissipation.

A brake caliper is mainly comprised of housing, brake pads, and pistons [12]. The housing is usually made of cast iron, the brake pads of semi-metallic, organic, and ceramic materials, and the pistons of plastic, aluminum, or chrome-plated steel. Generally, there

are two main types of brake calipers: the floating and the fixed calipers [25]. The calipers mostly differ in terms of design, mounting, and operation. On the one hand, the floating calipers move relative to the rotor. Furthermore, they have one or two pairs of pistons only on the inboard side of the rotor. When the brakes are applied, the fluid pressure moves the piston(s), which then pushes the entire caliper creating friction from the brake pads on both sides of the rotor. The floating calipers are prone to sticking failure resulted from dirt or corrosion at their moving components. This can cause extreme heating of the rotor, vehicle's steering vibration, and reduced fuel efficiency [26]. On the other hand, fixed calipers, as their name implies, do not move but are rather fixed with bolts to the caliper bracket. In addition, they have two to six pairs of pistons arranged on opposing sides of the rotor [12]. The fixed calipers, due to their multiple pairs of pistons, as well as their intricate brake fluid routing, have a more complicated geometry and are more expensive compared to the floating calipers. However, they are preferred for their performance because they have predictable braking behavior and due to the fact that their pads have balanced wear and less tapering [27].

In the rest part of this section, the fundamental formulas describing the kinetics and dynamics of a vehicle and its brake system are presented. The thermodynamics were neglected in this research work. Interested users should also be referred to the works of Milliken and Milliken [28], Heisler [24], and Jazar [29] for thorough details.

3.1. Brake System Kinetics

The main job of an automotive brake system is to slow down a vehicle by applying a friction force. Hence, the kinetic energy, $E_{kinetic}$, of the vehicle is converted to thermal energy, $E_{thermal}$, which in turn is absorbed by the brake system. A simplified formula describing the relation between a vehicle's mass with a given velocity and the difference in temperature of the brake system is the following [24]:

$$E_{kinetic} = E_{thermal}, \quad \frac{1}{2} m_v v_v^2 = m_{BS} c_{h,BS} \Delta T_{BS} \tag{4}$$

where

m_v: mass of the vehicle
v_v^2: velocity of the vehicle
m_{BS}: mass of the brake system
$c_{h,BS}$: specific heat capacity of the brake system
ΔT_{BS}: temperature change in the brake system

In a disc brake, the clamping force of the calipers to the brake discs is translated to a friction force opposing the disc's rotational direction and thus can be expressed by the equation:

$$F_{friction} = F_{clamping} * \mu \left(= \frac{M_b}{\mu * r_{eff}} * \mu \right) \tag{5}$$

where

$F_{friction}$: friction force on one wheel
$F_{clamping}$: clamping force
μ: friction coefficient between pad and disc
M_b: brake torque on the wheel
r_{eff}: effective pad radius
n: number of friction faces

The friction coefficient will be varied according to the applied pressure and temperature surface roughness connected to the wear. In addition, the moment of the disc is assumed constant throughout the rotating wheel assembly. In order to exploit the capabili-

ties of a braking system, the tire should be the limiting factor, and both the front and rear axles should be on the verge of locking. A mathematical expression of that is

$$m_v * g * \mu_{tire} = T_{limited} = m_v * g * z \quad (6)$$

where

$T_{limited}$: max wheel torque, given by the tire-ground friction coefficient and vehicle weight
μ_{tire}: friction coefficient between tire and ground
g: gravitational acceleration constant
z: deceleration proportional with g

The Formula (6) describes the maximum negative acceleration without exceeding μ_{tire}. In addition to the wheel torque, other parameters such as the aerodynamic drag, the drivetrain losses, the gear meshing, the oil viscosity, and the rolling resistance can contribute to the braking force [24].

3.2. Vehicle Dynamics

Three are the most applied models for the vehicle dynamics calculations that characterize its ride quality, such as vehicle's transmissibility, suspension travel, and tire deflection together with the tire-ground adhesion: the quarter car model, the 2-DOF half-car model, and the 4-DOF half-car model. These models are based on the following assumptions: rigid unsprung and sprung masses, linear suspension spring, and viscous damping. In addition, the tire in these models is represented as a combination of spring and damper. However, the tire damping is omitted in the analysis of all models [30]. The used models in this research work were the quarter car model and the 4-DOF half-car model.

The quarter-car model represents one-fourth of a vehicle. Its degrees of freedom are the translational displacement of both the sprung and unsprung mass, making it a 2-DOF model. Figure 2 illustrates a quarter-car model [29].

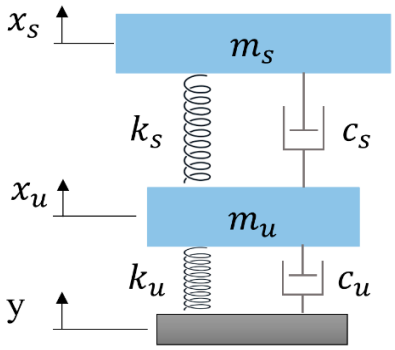

Figure 2. The quarter-car model, adapted from Jazar [29].

Here, the m_s and the m_u represent the quarter sprung and unsprung mass of a car, respectively. In addition, k_s, c_s represents the spring stiffness and damper coefficient of the shock absorber. Finally, k_u and c_u are the spring-damper effect of the tire. Both the sprung and the unsprung masses can be calculated by the following equations:

$$\text{Sprung mass}: \; m_s\ddot{x}_s = -k_s(x_s - x_u) - c_s(\dot{x}_s - \dot{x}_u) \quad (7)$$

$$\text{Unsprung mass}: \; m_u\ddot{x}_u = k_s(x_s - x_u) - c_s(\dot{x}_s - \dot{x}_u) - k_u(x_u - y) - c_u(\dot{x}_u - \dot{y}) \quad (8)$$

Translated into matrix form, we get the following equation of motion:

$$m\ddot{x} + c\dot{x} + kx = F \quad (9)$$

where

$$x = \begin{bmatrix} x_s \\ x_u \end{bmatrix}, m = \begin{bmatrix} m_s & 0 \\ 0 & m_u \end{bmatrix}, c = \begin{bmatrix} c_s & -c_s \\ -c_s & c_s + c_u \end{bmatrix} k = \begin{bmatrix} k_s & -k_s \\ -k_s & k_s + k_u \end{bmatrix}, F = \begin{bmatrix} 0 \\ k_u y + c_u \dot{y} \end{bmatrix}$$

This model was utilized for the calculation of the suspension vibration and helped the authors to identify the effect of a potential unsprung mass reduction in the case study of the racecar. However, this model takes into account only the bounce motion of the vehicle. For this reason, the 4-DOF half-car model was used in addition to the quarter-car model.

The 4-DOF half-car model was exploited for the pitch angle estimations, given the dynamic load distribution between the front and the rear axle and with regards to the front and rear braking load. At the 4-DOF half-car model depicted in Figure 3, the half body (m) of the car as well as one front (m_1) and one rear wheel (m_2) are presented. The k_{t1} and k_{t2} are the spring stiffness of the tires. Furthermore, c_1 and c_2 are the damping coefficients, and k_1 and k_2 the stiffness of the shock absorbers. Finally, the illustrated rigid bar in the model represents half of the car's mass, m, with a lateral moment of inertia, I_y.

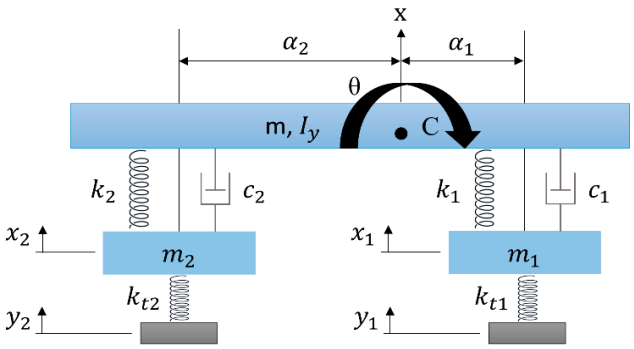

Figure 3. The 4-DOF half-car model adapted from Jazar [29].

The equation of motion from the quarter-car model, Equation (9), is used in this model too. However, in this case, the x, m, F, c, and k matrices are [29]:

$$x = \begin{bmatrix} x \\ \theta \\ x_1 \\ x_2 \end{bmatrix}, m = \begin{bmatrix} m & 0 & 0 & 0 \\ 0 & I_z & 0 & 0 \\ 0 & 0 & m_1 & 0 \\ 0 & 0 & 0 & m_2 \end{bmatrix}, F = \begin{bmatrix} 0 \\ 0 \\ y_1 k_{t1} \\ y_2 k_{t2} \end{bmatrix},$$

$$c = \begin{bmatrix} c_1 + c_2 & \alpha_2 c_2 - \alpha_1 c_1 & -c_1 & -c_2 \\ \alpha_2 c_2 - \alpha_1 c_1 & c_1 \alpha_1^2 + c_2 \alpha_2^2 & \alpha_1 c_1 & -\alpha_2 c_2 \\ -c_1 & \alpha_1 c_1 & c_1 & 0 \\ -c_2 & -\alpha_2 c_2 & 0 & c_2 \end{bmatrix},$$

$$k = \begin{bmatrix} k_1 + k_2 & \alpha_2 k_2 - \alpha_1 k_1 & -k_1 & -k_2 \\ \alpha_2 k_2 - \alpha_1 k_1 & k_1 \alpha_1^2 + k_2 \alpha_2^2 & \alpha_1 k_1 & -\alpha_2 k_2 \\ -k_1 & \alpha_1 k_1 & k_1 & 0 \\ -k_2 & -\alpha_2 k_2 & 0 & k_2 \end{bmatrix}$$

Both quarter-car and 4-DOF half-car models can be utilized as simplified representations of a vehicle's brake system. Furthermore, they can show that for constant spring stiffness and damping coefficient, a small increase of vehicle's mass will increase the total force, F. This will result in longer wheel travel and, thus, in an increasing damper frequency. The increased damper frequency, in turn, will lead to less tire-ground adhesion. A solution to the problem could be the increase of both damper coefficient and spring stiffness, but this can be managed with heavier components adding mass to the unsprung mass. Hence, the TO could be an alternative for the minimization of the vehicle's unsprung mass and the optimization of the braking system.

4. Methodology

In this research work, the development of front and rear brake calipers for a student racecar is presented. The in-house calipers were based on the commercial ISR calipers: the ISR 22-048 for the front caliper and the ISR-049 for the rear. Both are fixed calipers originally designed for 125cc bikes and Formula SAE racecars. However, the ISR 22-048 (front) uses four pistons while the ISR-049 (rear) two. The assemblies of the ISR calipers are illustrated in Figure 4.

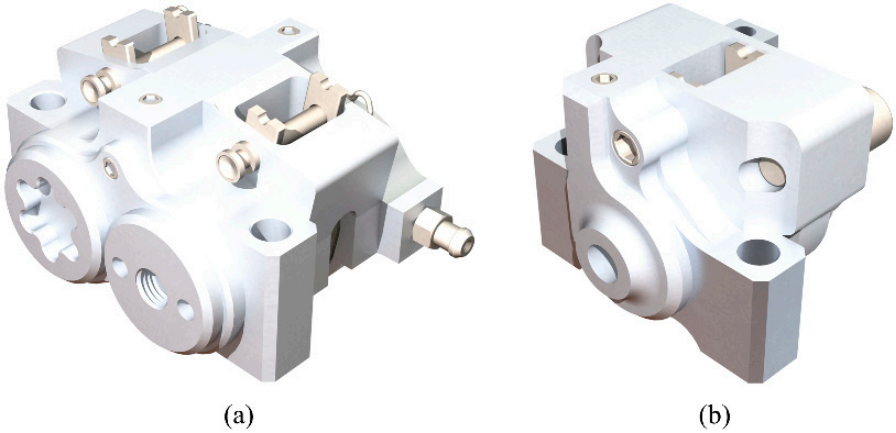

Figure 4. The ISR calipers in SolidWorks: (**a**) Front caliper and (**b**) Rear caliper.

At the beginning of this research, the identification of mass reduction possibilities was implemented. For this reason, an analysis of the vehicle's braking behavior, together with the ISR calipers, was conducted. Then, the calipers were optimized using a three-level optimization procedure in order to reduce their weight, and thus the total unsprung mass of the racecar. A reduction of the vehicle's unsprung mass could improve its performance. The implemented methodology is depicted in Figure 5.

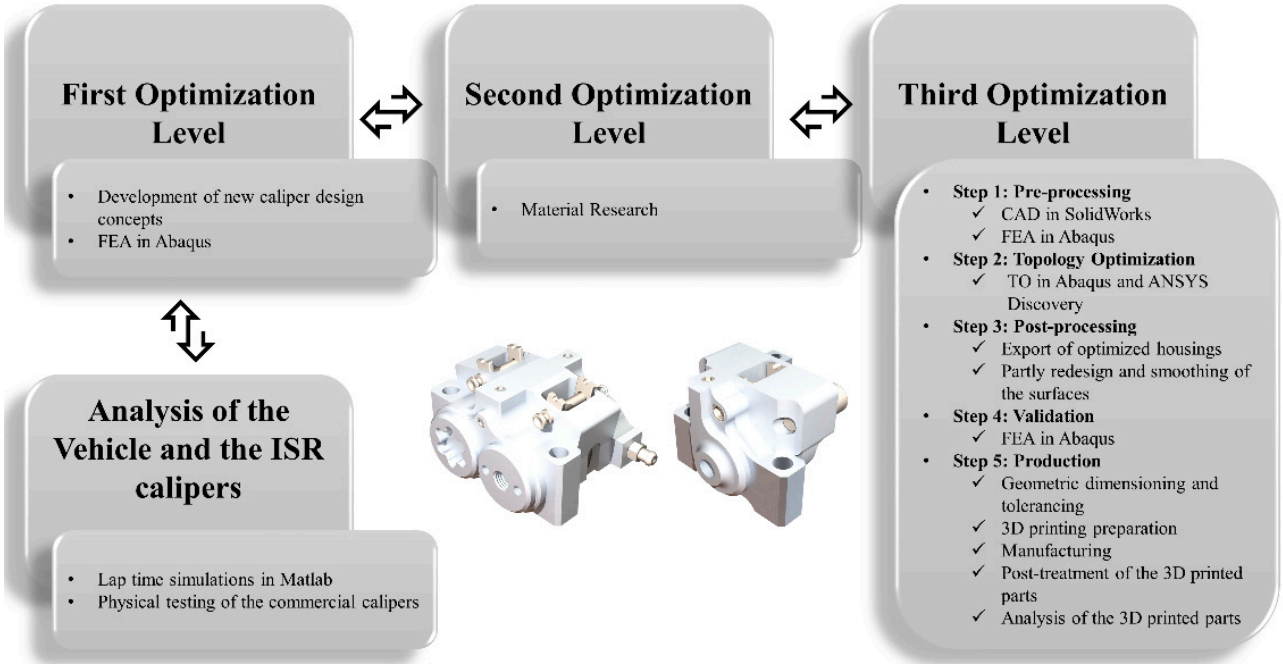

Figure 5. The optimization procedure.

The analysis of the vehicle and the ISR calipers comprises two main tasks: the lap time simulation of the vehicle in Matlab and the physical testing of the commercial ISR calipers using an in-house test jig.

The calipers were a part of the disc brakes of the racecar, which in turn were connected to a kinetic energy recovery system (KERS). The utilized KERS had limited torque output at the motor's top rpm. Thus, the vehicle's top speed was used as the dimension load. As has already been mentioned in Section 2, it is a good engineering practice to use the car tires as the limiting factor for the brake system. The chosen tires for the racecar were the Continental C19. A dynamic tire model was developed in MATLAB in order to conduct a lap time simulation. This model was based on the Continental's technical specifications and the Pacejka M5.2 tire model [31] and is given by the following tire formula:

$$y = D * \sin\left\{C * \tan^{-1}\left[B_x - E\left(B_x - \tan^{-1}(B_x)\right)\right]\right\} \quad (10)$$

where

y: force or moment resulting from a slip parameter
x: slip parameter
B: stiffness factor
C: shape factor
D: peak factor
E: curvature factor

Five lap time simulations were implemented for five different torques, range 300–700 Nm with a 100 Nm step. These simulations contributed to the calculation of the brake system's load case using the above tire model, the vehicle load transfer, as well as the aerodynamic- and motor representations. Furthermore, the minimum braking force that did not compromise the lap times was identified. Finally, the temperature development on the discs was estimated based on empirical data from previous autocross runs. These data were collected by an INFKL 800 °C IR brake temperature sensor placed into the hydraulic system of the disc brakes. Figure 6 depicts the results from the lap simulations of the calculated braking distance and velocity of the car and the distribution of the longitudinal forces, in the case of braking, from 120 km/h to 0 km/h. In addition, a temperature-time diagram is presented based on the sensor's data.

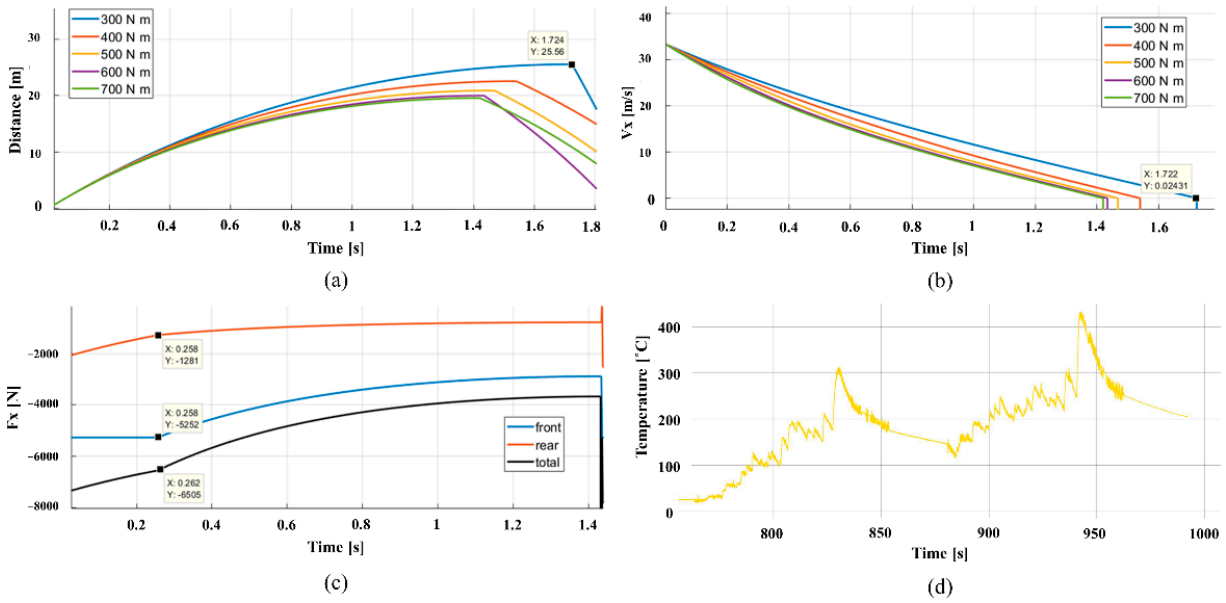

Figure 6. Braking from 120 km/h to 0 km/h: (**a**) Distance-time graph for different torques, (**b**) Velocity-time graph for different torques, (**c**) Longitudinal forces-time graph, and (**d**) Temperature-time graph.

The conducted simulations in Matlab showed a convergence of maximum brake force in cohesion to the tire model. Torque values above 600 Nm gave slower brake time as the brake force exceeds the tire's grip limit. In addition, from the longitudinal forces-time graph (graph c), it is observed that it is required a 0.8 brake balance between the front and the rear calipers. Finally, the empirical data of the temperature on the disc showed that a temperature up to 450 °C was expected on the disc brakes. According to Low [32], the main part of the generated heat, approximately 90–95%, is absorbed by the brake disc, and the rest 5–10% is distributed among the pads, the pistons, the brake fluid, and the caliper housing, assuming little to no heat dissipation. It is clear that the energy transferred during braking is highly related to the thermal resistance of the pads and the disc surface. Hence, the calipers also should be heat-resistant, and this is something that was taken into consideration in the choice of their production material.

The maximum allowed pressure on the brake master cylinder, according to their technical specifications, is 20 MPa. A pressure test was conducted at the ISR calipers, using an in-house test jig, and the maximum displacement in the y-direction of the front and the rear caliper, at 20 MPa, found 0.5 mm and 0.4 mm, respectively. In consequence, these were the maximum allowed displacements for the in-house developed calipers too. After the analysis of the vehicle and the ISR calipers, an optimization procedure of the calipers for their weight reduction was implemented on three levels, based on the Sudin, et al. [2] guidelines: downsizing of the vehicle, use of lighter materials in manufacturing, and removal of unwanted material from vehicle components.

At level one, new design concepts of the calipers were developed in SolidWorks by using reverse engineering of the commercial ISR calipers. The main goal at this point was either the reduction of the calipers' components or their downsizing. Thus, several design concepts were created and validated with respect to the ISR calipers' initial designs, the weight trade-offs among their components, and their interaction with the car's rim and upright. A crucial decision was to decrease the number of pistons from four to two in the front caliper. On the one hand, a four-piston caliper has an increased piston area and, thus, a reduced hydraulic pressure compared to a dual-piston caliper. However, the use of more pistons increases the risk of seal failure as well as the maintenance time. On the other hand, a dual-piston caliper could result in smaller design space and a less complex assembly due to the reduction of its components, but it contains a heavier housing to support its increased hydraulic pressure. Thus, there is a trade-off between the weight of the housing and the weight of the other caliper's components. The authors decided to develop a design concept of a dual-piston front caliper reducing its complexity and overall volume. Hence, both front and rear will be fixed dual-piston calipers. Furthermore, the initial design space of their housings was expanded as much as possible, with respect to the spatial placement of the wheel components, in order to increase the design flexibility for the TO algorithm. These design concepts, "design space assemblies", were validated in ABAQUS for the same load case and boundary conditions with the conducted physical test of the ISR calipers.

At the second level of optimization, an exploration of the material choices for the calipers was conducted. All the materials of the calipers' components, except the housings, were kept the same, thus from this point, the optimization focus was on housings only. It was decided that the optimized housings will be 3D printed using SLM. Hence, material research was done among the available 3D printing materials. Three were the predominant materials: AlSi10Mg, Steel MS1, and Ti6Al4V. On the one hand, the AlSi10Mg was the lightest material with the lowest specific gravity (2.7 g/cm^3) compared to the other two available options, the Steel MS1 (8.1 g/cm^3) and the Ti6Al4V (4.4 g/cm^3). Concerning the used case study in this paper, every gram counts in the development of calipers for a racecar. However, the calipers of a racecar are exposed to high braking forces and temperatures. Hence, the Ti6Al4V with an exceptional yield strength (1147 MPa), even at 500 °C (890 MPa), was considered an excellent choice [33].

Concerning the third optimization level, the housings of both front and rear calipers were topologically optimized, for weight reduction, without sacrificing their stiffness. The TO of the housings is divided into five steps; (1) Pre-processing, (2) Topology Optimization (TO), (3) Post-processing, (4) Validation, and (5) Production.

The pre-processing consists of the computer-aided design (CAD) of the housings in SolidWorks and the finite element analysis (FEA) of them in ABAQUS. The initial design concepts of the calipers' housings were created in SolidWorks with respect to the ISR brake calipers. The CAD files were exported and transferred to ABAQUS for FEA. The applied load case in the FEA was for maximum brake force at 120 km/h and warm tires. On the one hand, a pressure, P = 10 MPa, and surface traction, t = 7200 N, were applied at the pistons' area of the front housing. Furthermore, the housing was fixed with two bolts to the upright. These bolts were replaced in the simulations by two fixtures to reduce the simulation time. On the other hand, the pressure and the surface traction were P = 4 MPa and t = 2800 N, respectively, at the housing of the rear caliper. The same boundary conditions were also applied in this case. The design space, as well as the used forces and boundary conditions in both housings, are presented in Figure 7. The 3D models were discretized using 1 mm tetrahedral finite elements, resulted in 2,334,921 and 1,981,349 total elements for the front and the rear housing, respectively. The assigned material was an anisotropic Ti6Al4V with Young's modulus E_{XY} = 120 GPa and E_Z = 110 GPa, Poisson's ratio ν = 0.31, and density ρ = 4.41 g/cm^3. The material properties were taken from the EOS data sheet, which was the used material of the 3D printed housings.

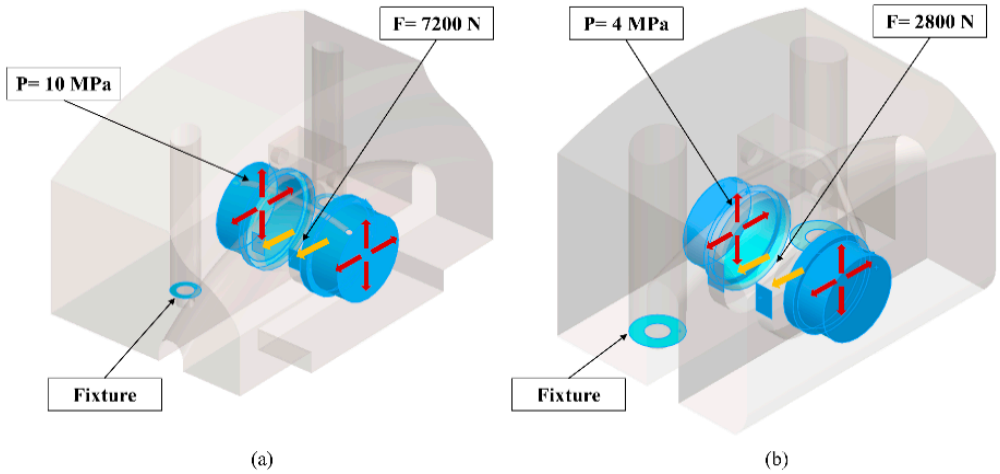

Figure 7. The design space, the loads, and the boundary conditions of the housings: (**a**) Housing of the front caliper, (**b**) Housing of the rear caliper.

Different TO software was used for the two case studies for comparison reasons. On the one hand, the housing of the front caliper was optimized with a condition-based algorithm in ABAQUS. This algorithm is based on the SIMP approach. The minimization of the model's strain energy was used as objective function while a volume fraction, equal to 7.45% of the initial design space, was used as function constraint. This volume fraction could lead to a 160 g housing. The 160 g target was set with regard to the targeted stiffness properties of the ISR caliper. Optimizing with volume constraints is a process of experimentation with different values of volume fraction until the stiffness goal is reached. Furthermore, the surfaces for the pistons and the fluid channel were the "frozen areas", and thus were excluded from the available design space. Finally, 300 design cycles were used as maximum limit. On the other hand, the housing of the rear caliper was optimized in ANSYS Discovery software. This software uses a sensitivity-based algorithm for the optimization and is GPU-based that promises automatically generated CAD models in less than an hour. The applied TO here was also the traditional compliance optimization where the minimization of strain energy was used again as objective function and the volume as

function constraint. However, in this case, the volume was set equal to 8.55% of the initial design space, which could lead to a 75 g housing. The surfaces for the pistons and the fluid channel were defined as frozen areas also here.

At the post-processing step, the optimized design solutions were imported as STL files to SolidWorks for redesign. Usually, the complex geometries of the optimized designs are making challenging their production with CPM. For this reason, a redesign procedure based on the optimized solutions takes place after the TO. However, when TO is oriented to AM, this step can be omitted. In this study work, it was decided to manufacture the housings with SLM 3D printing. Thus, the authors utilized the 3D printing flexibility and redesigned only the interacting surfaces and the crucial areas, such as the piston chambers, the seal surfaces, and the fluid channels. The latter was designed with a minimum angle equal to 30° in relation to the build plate in order to be free of support material. No tool could remove the support material inside the fluid channels. In addition, "power surfacing" was used in SolidWorks for the whole geometry. This feature smoothens the surface of the models and contributes to the mitigation of sharp areas that can lead to both stress concentrations and overhangs later in 3D printing. Finally, the optimized housings replaced their initial designs in the caliper assemblies. The assemblies were mirrored between the right and left wheel resulting in an equal force path on the left and right uprights. The symmetrical brake calipers can lead to a balanced brake performance of the vehicle.

The validation of the final designs was conducted in two steps. In the first step, only the housings of the calipers were checked with an FEA simulation similar to this at the pre-processing. Consequently, a second FEA simulation was implemented using assembly designs for the calipers. Each assembly consisted of a housing, two pistons, two bolts, a brake segment, and a foundation element acting as the upright. The brake pads were neglected from the validation studies to reduce the simulation time. However, the brake discs were made much thicker to compensate for the brake pads' thickness loss. This resulted in a load case of extremely worn brake pads. The used loads were: pretension of the bolts with bolt loads, F = 17 KN, the pressure inside the housing at the pistons' area, P = 16 MPa, and torque to the brake disc in normal driving direction, M_b = 600 Nm. On the other hand, the validation of the rear caliper was set with a pretension load F = 17 KN, a piston pressure P = 8 MPa, and a brake disc torque M_b = 300 Nm. Finally, the same boundary conditions were used in both cases, as they are shown in Figure 8.

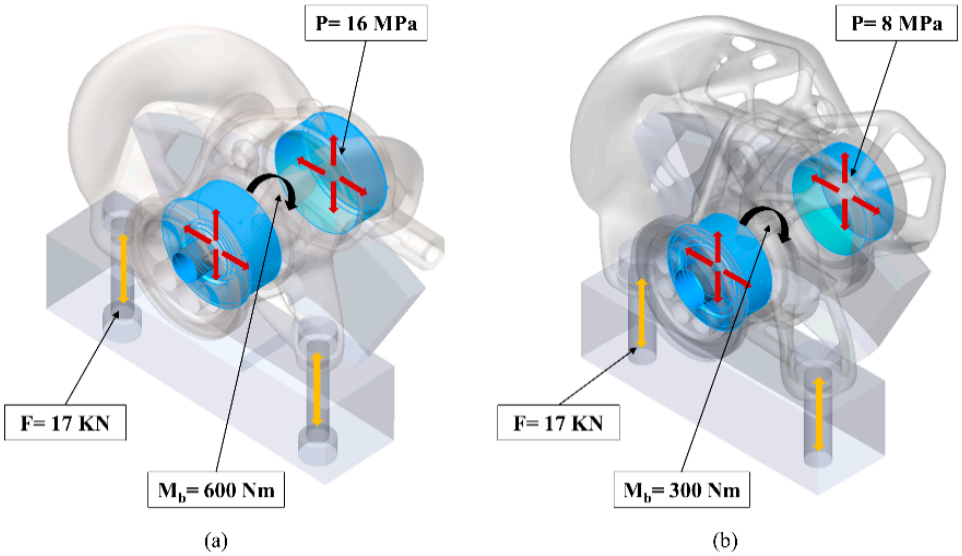

Figure 8. The used assemblies for the validation studies with their loads and boundary conditions: (**a**) Assembly of the front caliper, (**b**) Assembly of the rear caliper.

The final step in the presented methodology was the production of the calipers. Specifically, this step consists of five tasks, the geometric dimensioning and tolerancing, the 3D printing preparation, the manufacturing of the housings, and the post-treatment of the 3D printed parts as well as their analysis.

The possible post-machining process requires careful tolerancing and dimensioning of the housings, specifying the allowable deviations in both geometry, size, weight, and surface quality. Hence, technical drawings of the housings were developed based on ISO TC213. In addition, the interacting surfaces with the other components, such as the seals and the pistons, were designed according to the components' standards and specifications. For example, it is recommended that the pistons' surface finish should be 0.4 μm. That was noted in the technical drawings and will be measured later at the 3D printed parts.

As has been already mentioned, SLM 3D printing was chosen as a manufacturing method for both housings. Hence, a 3D printing preparation of the 3D models should be conducted. The support structure was used on features with more than a 30° overhang relative to the 3D printer plate. In addition, the fluid channels were free to support material. In general, additively manufactured models can suffer from poor surface finish and dimensional discrepancies making inevitable the post-machining of their surfaces interacting with other components such as bolts, bearings, and fitting parts. For this reason, the housings' surfaces that interact with the other caliper components were designed to be printed with 5 mm extra material.

Another challenge in 3D printing is that the 3D printed parts suffer from uneven material heating between their layers resulting in internal stresses and material anisotropy [34]. Hence, a 12-h curing process was conducted on the 3D printed parts at the post-treatment step. The housings were heat-treated at 740–900 °C over a period of up to 12 h for internal stress relaxation without any impact on their geometry [35]. After the curing process, the support material was removed from the housings.

Then, their weight and critical dimensions were measured in order to identify possible differences from the 3D models as well as post-machining needs. In addition, an in-house designed assembly jig and a test jig were developed for the assembly and the testing of the calipers. However, the post-machining of the housings, the assembly of the calipers, and their mechanical testing were planned for future work.

5. Results

The CAD designs and the bill of materials (BOM) of the caliper design concepts, developed at the first level of the optimization process, are depicted in Figure 9. Both calipers were dual-piston fixed calipers, and the size and number of their components were decreased, resulting in lighter design solutions. At this level, the weights of the front and rear caliper, except the housings, were 29.4% and 26.2% lighter than their commercial counterparts. On the other hand, the design space of their housings increased approximately five times comparing to the ISR housings, utilizing the maximum available space between the wheel, brake disc and surrounding suspension components. Hence, there was enough material for the TO conducted at the third optimization level. However, this increased the optimization time dramatically.

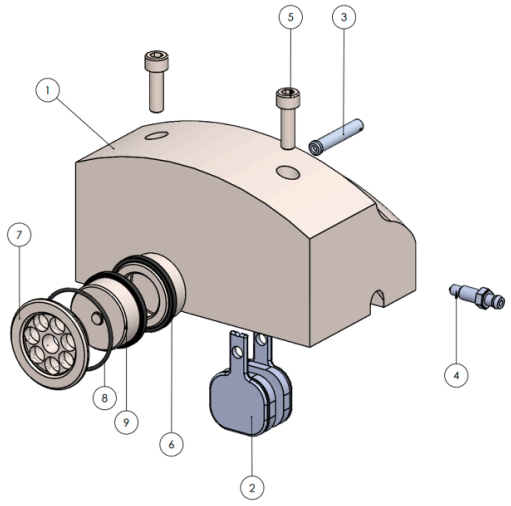

ITEM NO.	PART NAME	QTY.
1	Caliper Housing	1
2	Brake Pad	2
3	Pad Pin	1
4	Bleed Screw	1
5	Bolt - DIN 912 M6 x 20	2
6	Piston Ø30	2
7	End Cap Ø30	1
8	O-ring Ø36	1
9	Lip Seal Ø30	2

(a)

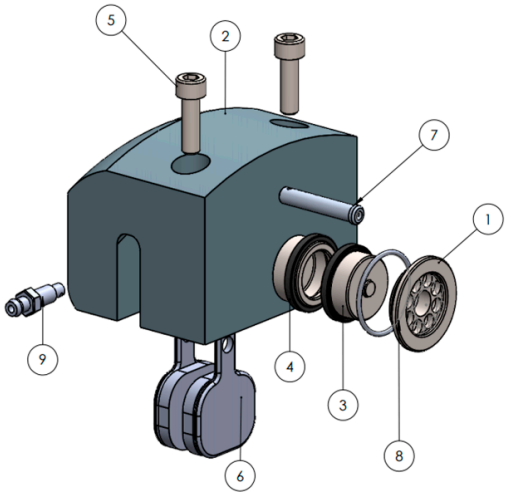

ITEM NO.	PART NAME	QTY.
1	End Cap	1
2	Caliper Housing	1
3	Piston Ø22	2
4	Lip Seal Ø22	2
5	Bolt - DIN 912 M6 x 20	2
6	Brake Pad	2
7	Pad Pin	1
8	O-ring Ø28	1
9	Bleed Screw	1

(b)

Figure 9. The assemblies of the caliper design concepts after the first optimization level in SolidWorks: (**a**) Front, (**b**) Rear.

The TO resulted in 42% and 64.7% weight reduction of the housings of the front and the rear caliper. The optimized geometry of the housings that was reconstructed in SolidWorks, resulted in a weight increase of 2.1% and 12.5%, respectively. This is something that was expected since both the partial redesign and the 3D printing preparation altered the initial geometries of the optimized results. However, the total weight of the front caliper was reduced to 36.9%, while the rear caliper was 48.5% lighter. The optimized 3D models of the housings are presented in Figure 10.

(a) (b)

Figure 10. The optimized housings in SolidWorks: (**a**) Front, (**b**) Rear.

The stress and displacement distribution at both housings and their assemblies, found by the validation studies, are depicted in Figures 11 and 12.

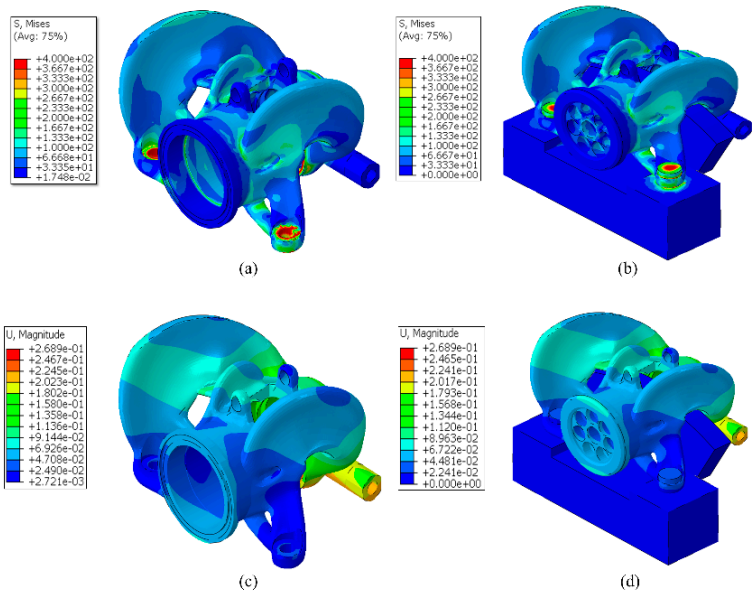

Figure 11. The results of the validation studies in ABAQUS for the front caliper: (**a**) Stress plot of the front housing, (**b**) Stress plot of the front caliper, (**c**) Total displacement of the front housing, (**d**) Total displacement of the front caliper.

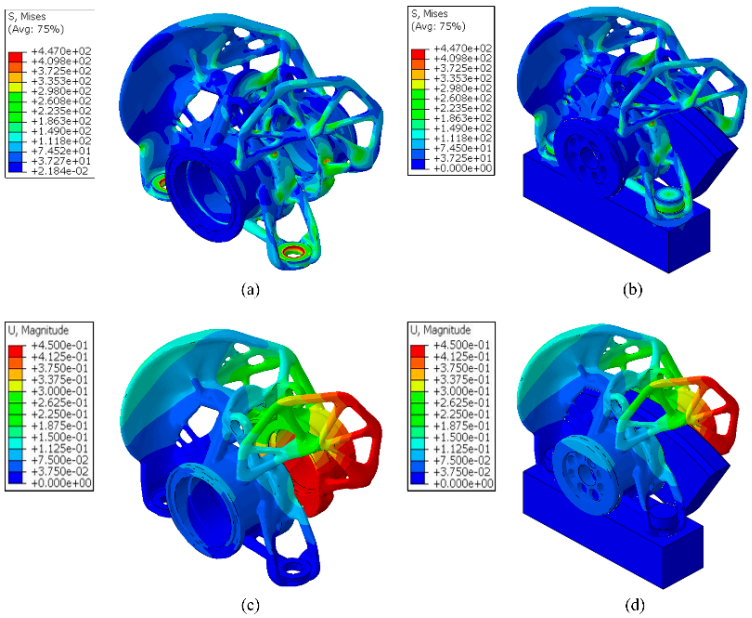

Figure 12. The results of the validation studies in ABAQUS for the rear caliper: (**a**) Stress plot of the rear housing, (**b**) Stress plot of the rear caliper, (**c**) Total displacement of the rear housing, and (**d**) Total displacement of the rear caliper.

The validation studies of both housings and calipers showed that the optimized housings were topologically optimized without sacrificing their stiffness. The validation studies of the assemblies were also utilized as a connectivity checking tool between the housings and the other components. On the one hand, the maximum stresses of the housings of the front and the rear caliper were 5.9% and 3.9% smaller than the ISR. Moreover, their maximum displacements were reduced by 59.3% and 17.1%, respectively. On the other hand, the optimized housings fit correctly to the calipers' assemblies. Furthermore, the

front caliper had a 400 MPa maximum stress while the rear caliper 447 MPa. Moreover, the displacements of both calipers were reduced. Specifically, the assemblies of the front and the rear caliper had a 50% and 17.5% reduction of their maximum displacement in y-direction compared to the ISR calipers.

The optimized housings were 3D printed at an EOS Lasertec 30 Dual SLM 3D printer in Ti6Al4V. Figure 13 depicts the 3D-printed parts on the building plate after the post-treatment. More components were printed for backup.

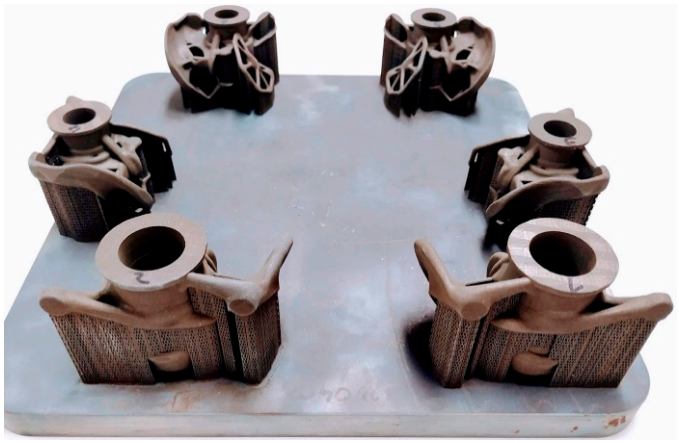

Figure 13. The 3D printed housings.

A weight deviation of both 3D printed housings was observed. In particular, the housing of the front caliper was 0.9% heavier than its 3D model, while the housing of the rear caliper was 6% heavier. Possible reasons for these differences could be the used tolerances of the STL files, especially on all part interacting surfaces, the insufficient removal of the support material, as well as remaining powder inside the 3D printed parts. Furthermore, a geometry comparison between the CAD models and the 3D printed parts was conducted using three basic dimensions, highlighted with arrows in Figure 14.

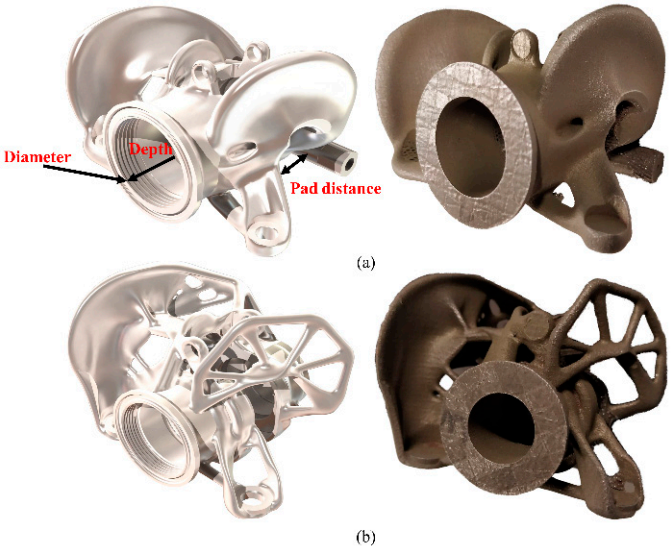

Figure 14. A geometry comparison between the CAD models and the 3D printed parts of the housings: (**a**) The front housing and (**b**) The rear housing.

The results are presented in Table 1 and showed small geometric deviations.

Table 1. Geometric deviations between the CAD models and the 3D printed parts of the housings.

	Diameter [mm]	Depth [mm]	Pad Distance [mm]
CAD of Front housing	25	59	10
3D printed Front housing	24.87	59.01	9.93
CAD of Rear housing	17	49.5	10
3D printed Rear housing	16.93	49.58	9.95
Average Deviation	−0.47%	0.09%	−0.60%

An overview of the results in this paper is presented in Table 2. In particular, the weights, the maximum stresses, and displacements of the ISR housings/calipers and the optimized housings/calipers are included.

Table 2. The results from the validation studies.

		Component/Assembly	Weight (g)	Max Stress (MPa)	Total Displacement (mm)	Displacement in Y (mm)
FRONT CALIPER	Housing	ISR 22-048	320	425	0.663	0.516
		Optimized (raw model)	185.75	434	0.47	0.39
		Optimized after redesign	189.64	400	0.27	0.25
		Optimized after 3D printing preparation	228.58	350	0.33	0.29
		3D printed	230.6	-	-	-
	Caliper	ISR 22-048 assembly	483	-	-	0.5
		Design space assembly	2285	73	0.041	0.037
		Optimized assembly	304.7	400	0.27	0.25
REAR CALIPER	Housing	ISR 22-049	210	465	0.543	0.461
		Optimized (raw model)	74.10	312	0.47	0.36
		Optimized after redesign	83.37	447	0.45	0.33
		Optimized after 3D printing preparation	112.4	405	0.37	0.36
		3D printed	119.2	-	-	-
	Caliper	ISR 22-049 Assembly	320.8	-	-	0.4
		Design space assembly	1254	44	0.012	0.009
		Optimized Assembly	165.11	447	0.45	0.33

6. Topology Optimization for Manufacturing

The TO is mainly used as a design tool. However, its utilization in manufacturing is possible but challenging. There are many parameters that should be taken into account, such as the overall optimization method, the manufacturing method as well as the TO approach, and its applied software.

The TO procedure is dependent on the overall optimization method and cannot be seen separately. The followed optimization method in this paper was implemented in three levels: the development of new caliper design concepts using less and downsized components, the exploration of lighter and stiffer materials in the production of the calipers' housings, and the removal of unwanted material from them by using TO. First, the modifications and changes made in the caliper assemblies could optimize the structures and save material without any loss in their performance. For example, the reduction of the pistons in the front caliper from four to two could reduce its weight. Secondly, material exploration was conducted for the housings. The AlSi10Mg was the lightest material among the available options; however, the Ti6Al4V was instead used due to its exceptional yield strength, even in high temperatures. In addition, the 3D printing preparation of the models should take into account the 3D printing material. For example, it is recommended

to use support material for an overhang angle bigger than 20–30° for titanium parts, while this angle limit is increased to 45° for parts made by aluminum. Third, the TO procedure focused on the housings, which were the heaviest components of the calipers. A small change in the overall optimization procedure could also have a high impact on the TO procedure. For example, the number and the spatial placement of the caliper's components could affect the design space of the housings, and thus the results of the conducted TO.

The manufacturing method of the housings has been decided from the beginning of this optimization work and was the SLM 3D printing. The reason for that was to avoid the time-consuming redesign step of the optimized solutions. This does not mean that the topologically optimized designs are only oriented to AM, but it highlights the need to redesign them before their manufacturing by CPM. When TO is oriented to 3D printing, the redesign at the post-processing of the design solutions can either be omitted or limited to the interacting surfaces and critical areas of the structure. Hence, topologically optimized designs can be manufactured directly or with small modifications. Moreover, a 3D printing preparation of the design should be committed, taking into account the 3D printing method, the use and removal of the support material, the 3D materials and their anisotropy, and possible needs for post-machining of the 3D printed parts. One example was the non-use of support material inside the fluid channel due to its impossible removal after 3D printing. Another example is the use of additional material on interacting surfaces. The 3D-printing parts suffer from poor surface finish making their post-machining inevitable in order to get good surface quality. Thus, the use of 5 mm extra material to the crucial surfaces created enough space for the surface finishing tools. Moreover, weight and dimensional deviation should be expected in 3D printing. Hence, the designer should take into account these deviations both in design and TO, introducing the required tolerances.

The used TO method in this paper was the traditional compliance TO with the SIMP as an interpolation method. According to the theory, the SIMP method does not consider material anisotropy. However, it is good practice to use the SIMP method due to its simplicity, and apply an anisotropic material to the structure. When the amount of the intermediate finite elements is small, a good approximation of the anisotropic properties can be achieved. However, it is important to notice that the created anisotropy is static and not design-dependent. For this reason, a deviation between the calculated and validated material properties of the 3D-printed parts should be expected.

The choice of the TO software affects the optimization time and the quality of the results. Concerning the TO software, both ABAQUS and ANSYS discovery led to interesting design solutions that respected the given optimization goals and restrictions. Concerning the optimization time, the optimization of the front housing with ABAQUS was completed after 295 design cycles and, thus, took many hours compared to the optimization of the rear housing in ANSYS discovery that was completed in less than an hour. On the one hand, ABAQUS with the TOSCA optimization module is one of the most traditional TO tools with a plethora of choices for both the optimization algorithms, the objective functions, the optimization constraints, as well as the load cases and the boundary conditions. In other words, for all possible designer choices [36]. On the other hand, the ANSYS discovery in this version (2020) is limited to simple load cases, basic constraints, and a sensitivity-based optimization algorithm that does not take the displacement of the structures into consideration, making it not ideal for multiple load cases and combined optimization goals. However, the software could cover the optimization needs of the rear caliper due to the used linear load case. Moreover, it offers real-time optimization in every design cycle, making the monitoring of the optimized results easier. ANSYS discovery live model predicted a 0.36 mm maximum displacement in the y-direction, which was close to the 0.33 mm displacement found in the validation study. It seems that its efficiency and accuracy as a GPU-based TO tool could be an interesting research topic in the future.

7. Conclusions

The optimization possibilities of a structure with a focus on its weight reduction were researched in this paper. The used case study was the brake calipers of a student racecar. The implemented optimization methodology in this research work could reduce the total weight of the supercar's calipers by approximately 668 g, which means a 41.6% weight reduction of the ISR calipers. Moreover, the maximum displacements of the calipers in the y-direction were also decreased by 50% and 17.5% for the front and the rear caliper, respectively. Hence, despite the fact that the produced calipers have not been tested yet, they were theoretically surpassing their commercial counterparts.

The weight optimization problem was confronted as a three-folded problem; using less and downsized components, applying lighter materials in production, and removing unwanted material. It is clear that the three levels of optimization could not be seen separately. The final designs with their technical details and the tolerances should take into account both the material selection and the production method. There is a big difference to design for the CPM and for AM. The use and the removal of the support material, the material anisotropy, the weight, and the dimensional deviations, especially in the interacting surfaces and the critical areas, should be taken into account when we design for 3D printing. There is a significant sensitivity in the optimization procedure. A small change either in the design parameters or in the 3D printings parameters can affect the final products and possibly lead to undesirable design solutions. However, when the TO for 3D printing are seen together with the CAD and the material choice, they can benefit the designer by providing remarkable material savings and complex design solutions that would have been impossible without TO. TO can be used as a tool for design inspiration. However, with the appropriate procedure and parameters, the topologically optimized designs can be manufactured and used. A designer should decide between the possible identified trade-offs in an optimization process, such as the material selection, the TO for CMP with a full redesign or TO for AM with a 3D printing preparation, the design space versus the simulation time, as well as the choice among the different TO methods and software. However, he/she should consider the TO not only as an optimization tool but also as a design and a CAM tool. Designers interested in optimization methods, such as TO, and in automotive production could exploit the findings of this paper.

8. Future Research

The post-machining of the 3D printed housings, the assembly of the calipers as well as the mechanical testing of them at the in-house jigs will take place in the near future. In addition, the installation of temperature sensors into the hydraulic system of the brakes could collect essential data related to the brake system's behavior under high temperatures and calculate real discs and pad wear. The findings from these procedures could create a more accurate picture of the possible load scenarios and contribute to further development of the calipers with a broader materials selection and design concepts. New design concepts can be explored in the design phase, such as single-piston calipers or calipers with different bolt patterns that could lead to additional weight savings. Moreover, alternative TO methods, such as lattice optimization, can be applied in seek of the lightest calipers. The lattice optimization could exploit more of the advantages of AM, resulting in even stiffer and lighter parts. Finally, the identification of all the parameters that should be taken into account in the TO procedure and affect the manufactured parts could lead to a more automatic TO procedure, oriented towards manufacturing.

Author Contributions: Conceptualization, M.L. and E.T.; methodology, M.L. and E.T.; software, M.L.; writing—original draft preparation, E.T.; writing—review and editing, E.T.; supervision, M.S.; All authors have read and agreed to the published version of the manuscript.

Funding: This research received no external funding.

Institutional Review Board Statement: Not applicable.

Informed Consent Statement: Not applicable.

Data Availability Statement: Not applicable.

Conflicts of Interest: The authors declare no conflict of interest.

References

1. Li, C.; Kim, I.Y.; Jeswiet, J. Conceptual and detailed design of an automotive engine cradle by using topology, shape, and size optimization. *Struct. Multidiscip. Optim.* **2015**, *51*, 547–564. [CrossRef]
2. Sudin, M.N.; Tahir, M.M.; Ramli, F.R.; Shamsuddin, S.A. Topology optimization in automotive brake pedal redesign. *Int. J. Eng. Technol. (IJET)* **2014**, *6*, 398–402.
3. Bendsøe, M.P.; Sigmund, O. *Topology Optimization: Theory, Methods, and Applications*; Springer: Berlin, Germany; New York, NY, USA, 2003; p. xiv. 370p. [CrossRef]
4. Tyflopoulos, E.; Flem, D.T.; Steinert, M.; Olsen, A. State of the art of generative design and topology optimization and potential research needs. In *DS 91: Proceedings of NordDesign 2018, Linköping, Sweden, 14–17 August 2018 Design in the Era of Digitalization*; The Design Society: Glasgow, UK, 2018; p. 15.
5. Yang, R.; Chahande, A. Automotive applications of topology optimization. *Struct. Optim.* **1995**, *9*, 245–249. [CrossRef]
6. Shin, J.-K.; Lee, K.-H.; Song, S.-I.; Park, G.-J. Automotive door design with the ULSAB concept. using structural optimization. *Struct. Multidiscip. Optim.* **2002**, *23*, 320–327. [CrossRef]
7. Li, G.; Xu, F.; Huang, X.; Sun, G. Topology optimization of an automotive tailor-welded blank door. *J. Mech. Des.* **2015**, *137*. [CrossRef]
8. Kong, Y.; Abdullah, S.; Omar, M.Z.; Haris, S.M. Topological and topographical optimization of automotive spring lower seat. *Lat. Am. J. Solids Struct.* **2016**, *13*, 1388–1405. [CrossRef]
9. Li, C.; Kim, I.Y. Multi-material topology optimization for automotive design problems. *Proc. Inst. Mech. Eng. Part. D: J. Automob. Eng.* **2018**, *232*, 1950–1969. [CrossRef]
10. Cavazzuti, M.; Baldini, A.; Bertocchi, E.; Costi, D.; Torricelli, E.; Moruzzi, P. High performance automotive chassis design: A topology optimization based approach. *Struct. Multidiscip. Optim.* **2011**, *44*, 45–56. [CrossRef]
11. Mastinu, G. Brake development methods—Topology optimization of a brake caliper and upright of a race car. In Proceedings of the 7th the International Munich Chassis Symposium, Munich, Germany, 14–15 June 2016; pp. 655–668.
12. Ballo, F.M.; Gobbi, M.; Mastinu, G.; Pishdad, A. Lightweight design of a brake caliper. In Proceedings of the ASME 2013 International Design Engineering Technical Conferences and Computers and Information in Engineering Conference, Portland, OR, USA, 4–7 August 2013; p. V001T001A010. [CrossRef]
13. Farias, L.T.; Schommer, A.; Haselein, B.Z.; Soliman, P.; de Oliveira, L.C. *Design of a Brake Caliper using Topology Optimization Integrated with Direct Metal. Laser Sintering, 24th SAE Brasil International Congress and Display*; SAE International: Warrendale, PA, USA, 2015; ISSN 0148-7191.
14. Soh, H.; Yoo, J. Optimal shape design of a brake calliper for squeal noise reduction considering system instability. *Proc. Inst. Mech. Eng. Part. D J. Automob. Eng.* **2010**, *224*, 909–925. [CrossRef]
15. Sergent, N.; Tirovic, M.; Voveris, J. Design optimization of an opposed piston brake caliper. *Eng. Optim.* **2014**, *46*, 1520–1537. [CrossRef]
16. Zhu, J.; Zhou, H.; Wang, C.; Zhou, L.; Yuan, S.; Zhang, W. A review of topology optimization for additive manufacturing: Status and challenges. *Chin. J. Aeronaut.* **2021**, *34*, 91–110. [CrossRef]
17. Christensen, P.W.; Klarbring, A. *An Introduction to Structural Optimization*; Springer Science & Business Media: Linköping, Sweden, 2008; Volume 153. [CrossRef]
18. Bendsøe, M.P. Optimal shape design as a material distribution problem. *Struct. Optim.* **1989**, *1*, 193–202. [CrossRef]
19. Allaire, G.; Cavallina, L.; Miyake, N.; Oka, T.; Yachimura, T. The homogenization method for topology optimization of structures: Old and new. *Interdiscip. Inf. Sci.* **2019**, *25*, 75–146. [CrossRef]
20. Razvan, C. Overview of structural topology optimization methods for plane and solid structures. *Ann. Univ. Oradea Fascicle Manag. Technol. Eng.* **2014**, *23*, 1583–1591. [CrossRef]
21. Bendsøe, M.P.; Kikuchi, N. Generating Optimal Topologies in Structural Design Using a Homogenization Method. *Comput. Methods Appl. Mech. Eng.* **1988**, *71*, 197–224. [CrossRef]
22. Bhandari, V. *Design of Machine Elements*; Tata McGraw-Hill Education: New Delhi, India, 2010.
23. Tyagi, P. Finite Element Analysis of Innovated Design of Racing Brake Calipers. Ph.D. Thesis, Department of Mechanical Engineering, College of Engineering, Wichita State University, Wichita, KS, USA, 2006.
24. Heisler, H. *Advanced Vehicle Technology*; Elsevier: Amsterdam, The Netherlands, 2002.
25. Phad, D.; Auti, T.; Joshi, R.; Jadhav, S.; Devasthali, S. Design and Analysis of a Brake Caliper. *Int. J. Automob. Eng.* **2015**, *5*, 2277–4785.
26. Matsushima, T.; Masumo, H.; Ito, S.; Nishiwaki, M. FE Analysis of Low-frequency Disc. Brake Squeal (In Case of Floating Type Caliper). In Proceedings of the 4th International Colloquium, ICGI-98, Ames, IA, USA, 12–14 July 1998; p. 327, ISSN 0148-7191. [CrossRef]

27. Kashyap, P.K.; Arya, D.; Gupta, K.; Kumar, K.; Khan, M.S. Design and Analysis of Single Piston Floating Brake Caliper. *Int. J. Eng. Res. Technol.* **2019**, *8*, 910–916.
28. Milliken, W.F.; Milliken, D.L. *Race Car Vehicle Dynamics*; Society of Automotive Engineers: Warrendale, PA, USA, 1995; Volume 400.
29. Jazar, R.N. *Vehicle Dynamics: Theory and Application*, 1st ed.; Springer: New York, NY, USA, 2017; pp. 217–575.
30. Talukdar, S.; Mazumdar, A.; Mullasseril, M.; Kalita, K.; Ujjwal, A. *Mathematical Modeling in Vehicle Ride Dynamics, SAE 2012 World Congress & Exhibition, Michigan, USA, 24–26 April 2012*; SAE International: Warrendale, PA, USA, 2012; ISSN 0148-7191. [CrossRef]
31. Pacejka, H.B.; Bakker, E. The magic formula tyre model. *Veh. Syst. Dyn.* **1992**, *21*, 1–18. [CrossRef]
32. Low, I.-M. *Ceramic-Matrix Composites: Microstructure, Properties and Applications*; Woodhead Publishing: Cambridge, UK, 2006.
33. Qian, M.; Froes, F.H. *Titanium Powder Metallurgy: Science, Technology and Applications*; Butterworth-Heinemann: Oxford, UK, 2015.
34. Chen, L.; Huang, J.; Lin, C.; Pan, C.; Chen, S.; Yang, T.; Lin, D.; Lin, H.; Jang, J. Anisotropic response of Ti-6Al-4V alloy fabricated by 3D printing selective laser melting. *Mater. Sci. Eng. A* **2017**, *682*, 389–395. [CrossRef]
35. Zguris, Z. How mechanical properties of stereolithography 3D prints are affected by UV curing. *Inc. Somerv. MaAccessed Mar.* **2016**, *7*, 2017.
36. Tyflopoulos, E.; Steinert, M. Messing with boundaries-quantifying the potential loss by pre-set parameters in topology optimization. *Procedia CIRP* **2019**, *84*, 979–985. [CrossRef]